J Mater Sci: Mater Electron (2021) 32:18163–18177

Synthesis, physical, linear optical and nuclear radiation shielding characteristics of B_2O_3–BaO–PbO–SrO_2 glasses

A. S. Abouhaswa[1,2], H. O. Tekin[3,4], Emad M. Ahmed[5], O. Kilicoglu[6], and Y. S. Rammah[1,*]

[1] *Department of Physics, Faculty of Science, Menoufia University, Shebin El-Koom, Menoufia 32511, Egypt*
[2] *Institute of Natural Science and Mathematics, Ural Federal University, Ekaterinburg 620002, Russia*
[3] *Medical Diagnostic Imaging Department, College of Health Sciences, University of Sharjah, 27272 Sharjah, United Arab Emirates*
[4] *Medical Radiation Research Center (USMERA), Uskudar University, 34672 Istanbul, Turkey*
[5] *Department of Physics, College of Science, Taif University, P.O. Box 11099, Taif 21944, Saudi Arabia*
[6] *Nuclear Technology and Radiation Safety Department, Vocational School of Health Services, Uskudar University, 34672 Istanbul, Turkey*

Received: 18 April 2021
Accepted: 7 June 2021
Published online:
17 June 2021

ABSTRACT

In the present work, the physical, UV–Vis–NIR spectroscopy, and nuclear shielding properties of novel borate glasses with nominal compositions $50B_2O_3$–25BaO–25PbO–$xSrO_2$: x = 0–30 mol% (BBPS0–BBPS30) have been investigated. The non-crystalline nature of the fabricated glasses was verified utilizing X-ray diffraction (XRD) measurements. Direct and indirect (E_{gap}^{Direct}, $E_{gap}^{Indirect}$) optical energy gaps, average of refractive index (n), Urbach's energy for (BBPS0–BBPS30) glasses were determined. MCNPX simulation code and WinXCOM program were employed to evaluate the mass attenuation coefficient, half value layer, tenth value layer, mean free path, and effective atomic number (μ_m, HVL, TVL, MFP, and Z_{eff}) of gamma for the proposed glasses. Neutron shielding survey was examined by determining neutron removal cross section (NRCS, ΣR) of glasses. Results reveal that E_{gap}^{Direct} varied from 3.15 to 2.38 eV, while $E_{gap}^{Indirect}$ from 3.07 to 2.28 and n from 2.268 to 2.606 for BBPS0 and BBPS30 glasses, respectively. The HVL, MFP, and TVL values corresponding to the materials were in a descending order BBPS0 > BBPS5 > BBPS10 > BBPS15 > BBPS20 > BBPS30. Therefore, the BBPS30 has superior shielding features against gamma-rays than the other material in the studied sample of glasses.

Address correspondence to E-mail: dr_yasser1974@yahoo.com

https://doi.org/10.1007/s10854-021-06359-7

1 Introduction

In last decades, heavy metal oxide (HMO) based glasses have gained significant attention due to their unique interesting electrical, optical, and magnetic properties. Additionally, these glasses have large exciton binding energy (BE) and wide bandgap. These properties make HMO based glasses potential candidates in several applications such as UV-emitting lasers, optoelectronic devices, gas sensors, and solar energy converters and gas sensors [1]. Boric oxide (B_2O_3) is an attractive oxide among the HMOs since it is one of the most common glass formers. Borate glasses exhibit more desirable physical and chemical properties, including a low melting point, strong clarity, chemical resistance, and thermal stability [1, 2]. Additionally, owing to their motivating nonlinear and linear optical properties, borate glasses of various compositions play a significant role in optical devices [3–12]. Through incorporating lead oxide into borate glass structures, such properties such as optical nonlinearity may be enhanced due to the strong polarizability of Pb2 + ions in glass networks [13]. Environments of Pb cations in oxide glasses have been also probed by X-ray studies [14]. On the other side, the interaction of PbO and B_2O_3 in the glass matrix has a dual impact on the glass network, acting as a glass former in the presence of high levels of boron oxide or lead oxide and as a network modifier at low concentrations. Thus, lead borate glasses exhibit a wide glass forming range, which is advantageous for the fabrication of structurally and optically diverse structures [15–17]. On the other hand, Lead borate glasses are known to be excellent candidate materials for optoelectronic, photoelectric, and optical switches for the reasons mentioned previously. The additive of alkaline earth oxides namely BaO or/and SrO into borate glass structure allows to increase the glass refractive index and thermal stability. Previously, Manikandan et al. [18] investigated effect of BaO on the optical and thermal properties of some tellurite glasses. The authors confirmed that optical properties of glasses were enhanced with increasing BaO content in their compositions. In addition, they reported that thermal stability of glasses improved with increasing BaO concentration making these glasses with BaO attractive candidates for amplifiers in the mid-IR and fiber lasers [9]. In other study, Elkhoshkhany et al. [19] evaluated structural properties, UV–Vis–NIR spectroscopy and thermal characteristics of oxyhalide–tellurite glasses with $SrCl_2$. They reported that glass systems with Sr have high thermal stability and high index of refraction that makes them suitable as attractive candidates for optical fiber production. Recent research has shown that glasses are suitable for use as radiation filters owing to their unique properties, including their transparency to visible light and their capacity to absorb X-rays and neutrons [20]. By incorporating oxides into the glass matrix, the properties of the glasses against nuclear radiation shielding may be improved [21, 22]. Numerous scholars asserted that borate glasses continue to be the best option for radiation protection [10, 23–29]. The mass attenuation coefficient is the most useful gamma-ray attenuation parameter for evaluating the radiation shielding capability of materials. Numerous techniques, including Monte Carlo simulations and theoretical estimates using the XCOM and Phy-X/PSD systems, can be used to approximate the mass attenuation coefficients (MAC) [10, 26–31].

The main objective of this study is to determine potential synergistic effects of increasing SrO_2 additive on B_2O_3–BaO–PbO–SrO_2 glass system. To observe the direct effects of utilized chemical substitutions (i.e., B_2O_3/SrO_2), MAC of glass samples were determined in this analysis using an experimental transmission setup. The obtained findings were compared to those obtained by Monte Carlo simulations (MCNPX v.2.6.0) and theoretical calculations (WinXcom program). The obtained MAC values were used to quantify other critical shielding parameters, including linear attenuation coefficients (LAC), half value layer (HVL), mean free path (MFP), tenth value layer (TVL), and effective atomic numbers (Z_{eff}), as well as fast neutron removal cross sections values for novel lead–borate glasses. Along with their protecting properties against nuclear radiation, the physical and optical properties of the prepared glasses were studied.

2 Experimental and methods

2.1 Materials and measurements

By utilization of traditional and well-known method namely melt-quenching technique, commercial powders of high reagent grade of B_2O_3 of purity 99.96% Sigma-Aldrich, $BaCO_3$ of purity 99.99% Sigma-

Table 1 Chemical composition, density, and molar volume of the $(50-x)B_2O_3$–$25BaO_3$–$25PbO$–$xSrO_2$: x = 0–30 mol% glasses

Sample code	Chemical composition				Density gm/cm^3	Molar volume (cm^3/mol)
	B_2O_3	BaO	PbO	SrO_2		
BBPS0	50	25	25	0	4.685	27.522
BBPS5	45	25	25	5	4.790	27.441
BBPS10	40	25	25	10	4.895	27.363
BBPS15	35	25	25	15	5.000	27.288
BBPS20	30	25	25	20	5.105	27.216
BBPS30	20	25	25	30	5.315	27.082

Aldrich as a source of BaO, PbO of purity 99.9% Sigma-Aldrich, and SrO_2 of purity 99.99% Sigma-Aldrich were utilized to synthesis samples of lead borate glasses series with the compositions:

$50B_2O_3$–25BaO–25PbO–$0SrO_2$ coded as **BBPS0,**
$45B_2O_3$–25BaO–25PbO–$5SrO_2$ coded as **BBPS5,**
$40B_2O_3$–25BaO–25PbO–$10SrO_2$ coded as **BBPS10,**
$35B_2O_3$–25BaO–25PbO–$15SrO_2$ coded as **BBPS15,**
$30B_2O_3$–25BaO–25PbO–$20SrO_2$ coded **BBPS20,** and
$20B_2O_3$–25BaO–25PbO–$30SrO_2$ coded as **BBPS30.**

For each glass sample, the required weights of chemical powers were determined by an electric digital balance with accuracy of ± 0.0001. Next, they mixed well and melted in a porcelain-crucible at 950 °C for 25 min. Next, the melt-liquid was poured into preheated molds. The produced glass samples were annealed for 5 h at 300 °C to erase thermal strains and then left to cool down gradually. The produced glasses were polished well to make the two opposite faces parallel and flat to be ready for the optical measurements. The details of manufactured glasses with their sample codes and compositions are presented in Table 1. On the other hand, manufactured samples with their general appearance are shown in Fig. 1. Shimadzu 7000 diffractometer device with Cu a radiation source (λ = 1.54060 Å) in the 2θ range of 10°–100° was used to perform the XRD of the glass samples to examine the state of the prepared glasses. Densities of the prepared samples measured by Archimedes' technique using toluene (density, ρ = 0.867 g/cm^3) as liquid for immersion with accuracy of ± 0.01 g/cm^3 through the following Eq. (1):

$$\rho_{glass} = \frac{W_1}{W_1 - W_2}\rho_{toluene}. \quad (1)$$

Here,
W_1 = glass's weight in air.
W_2 = glass's weight in liquid.
$\rho_{toluene}$ = toluene liquid's density.

Molar volume (V_m) of each glass was calculated using Eq. (2):

$$V_m = \frac{M_{Wglass}}{\rho_{glass}}. \quad (2)$$

The optical absorption measurements for the (BBPS0–BBPS30) were carried out and drawn in wavelength from 190 to 1100 nm range by utilizing UV–Vis–NIR spectrophotometer of JASCO model V-570.

2.2 Methods

2.2.1 *Monte Carlo simulations*

The value of mathematical simulation methods in studies of nuclear radiation shielding remains a hot topic in the literature. Numerous scenarios are

Fig. 1 An image of the prepared BBPS0–BBPS30 glass samples

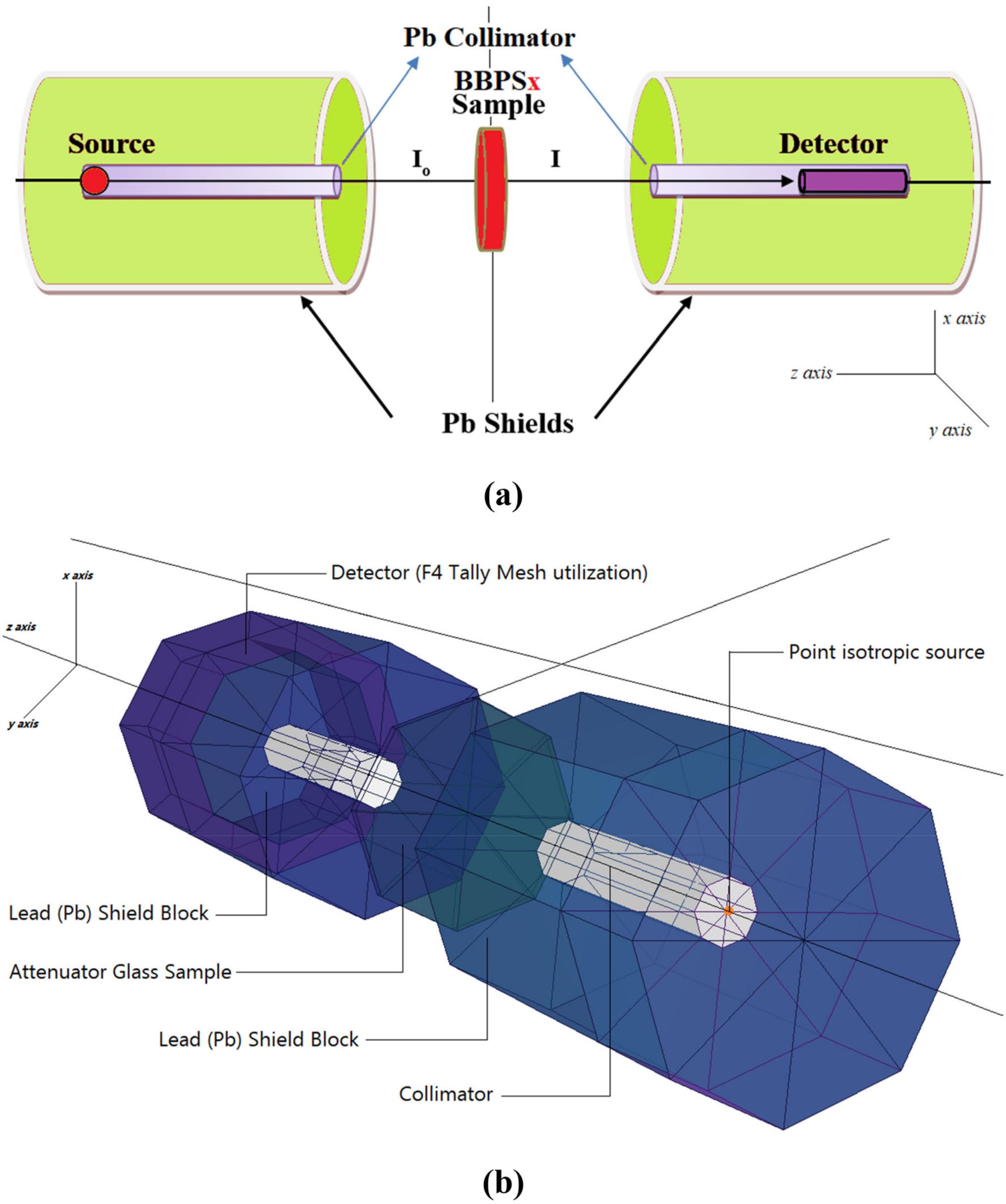

Fig. 2 **a** Simulation setup for MAC calculations **b** 3-D view of modeled simulation setup in MCNPX code (MCNPX Visual Editor)

possible during numerical simulation, based on the characteristics and features of the running code. The section on Monte Carlo simulations will explore the technological aspects of Monte Carlo simulations utilizing the MCNPX [32] code. Each glass sample was modeled in this study using elemental mass fractions and densities (Table 1). Material definitions for fabricated composites encoded as BBPS0, BBPS5, BBPS10, BBPS15, BBPS20, and BBPS30 were entered into the MCNPX code's input register. The MCNPX's substance description (M_n) entails many critical definition measures, including elemental mass fractions, atomic numbers, and mass numbers of components. Figure 2a–b illustrates the overall presence of the modeled simulation setup with the simulation package used to calculate mass attenuation and

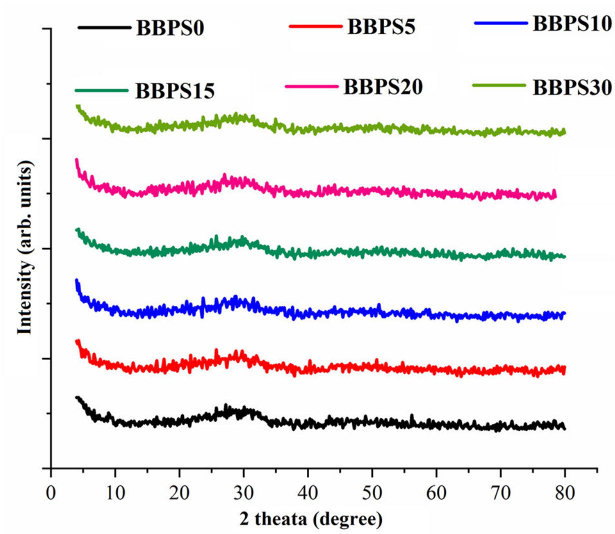

Fig. 3 XRD patterns of BBPS0–BBPS30 glass samples

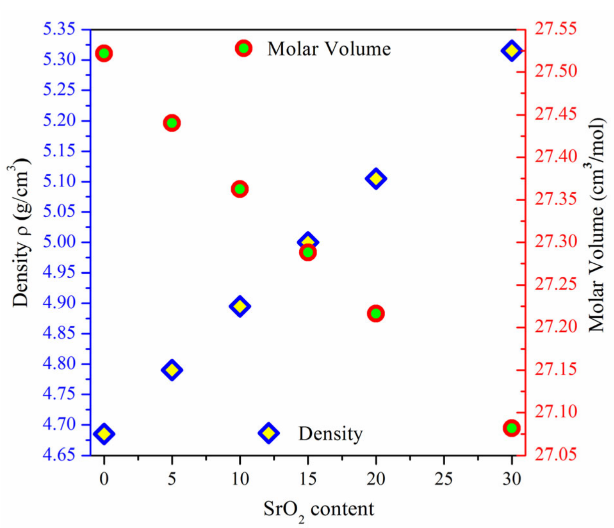

Fig. 4 Density and molar volume of BBPS0–BBPS30 glasses

transmission variables. Finally, one of the detection tallies encoded in MCNPX code (F4 tally mesh) was implemented within the virtual detection area to record the attenuated rays from the glass samples. It should be remembered that the MCNPX simulations were run for each glass sample at various photon energies. As a physics library, the D00205ALLCP03 MCNPXDATA kit was introduced, which consisted of DLC-200/MCNPDATA.

2.2.2 μ/ρ, HVL, and MFP, and Z_{eff}

The total mass attenuation coefficient ($\mu_m = \mu/\rho$, usually in cm^2/gram) is a fundamental concept used to describe the potential of a substance (in this case, Goethite glasses) to attenuate gamma radiation. Numerous methods, like XCOM, MCNP, Xmudat, and Geant4, may be used to obtain the _m factor. Fortunately, both of these techniques are based on the mixture law, as described in [33]:

$$\frac{\mu}{\rho} = \mu_m = \frac{N_A}{M}\sigma_{tot} = \sum_i w_i(\mu/\rho)_i \quad (3)$$

w_i denotes the weight fraction of the ith material contained in the glass sample. The μ_m values for Goethite glasses were obtained in our work using the XCOM software. Other shielding terms such as transmitting factors (e.g., MFP and HVL) and Z_{eff} were then calculated using the following equations [34, 35]:

$$\mathrm{MFP} = {}^{1}\!/_{\mu} \quad (4)$$

$$\mathrm{HVL} = (\ln 2/\mu) \quad (5)$$

$$Z_{eff} = \frac{\sigma_a}{\sigma_e} = \frac{\sum_i f_i A_i \left(\frac{\mu}{\rho}\right)_i}{\sum_j f_j \frac{A_j}{Z_j}\left(\frac{\mu}{\rho}\right)_j} \quad (6)$$

3 Results and discussion

3.1 XRD and physical parameters

XRD spectra for fabricated glasses BBPS0–BBPS30 don't illustrate any crystalline peaks as presented in Fig. 3, which confirm that glasses are in the amorphous nature.

Equation 1 and Eq. 2 were used to evaluate ρ_{glass} and the corresponding V_m. The obtained data are collected in Table 1 and depicted in Fig. 3. From Table 1 and Fig. 4, one can observe that ρ value raises from 4.685 to 5.315 g/cm^3 with increasing SrO_2 content in the proposed glasses. This increasing in ρ_{glass} may be due to the partial replacement between the light B_2O_3 with molar mass (69.63 g/mol) and heavy SrO_2 with molar mass of (119.619 g/mol). The V_m decrease with increasing SrO_2 content in the proposed glasses as in Table 1 and Fig. 3. This decreasing may be attributed to (i) the amount of B_2O_3 with shorter atomic radii (1.589 Å) was larger than that of SrO_2 with longer atomic radii (4.303 Å) and (ii) the number of NBO decreases with decrease B_2O_3

making glasses in less inter-atomic spacing and disordered formation.

3.2 UV–Vis spectroscopy and optical properties

The UV–vis spectra for BBPS0–BBPS30 glasses are illustrated in Fig. 5. It is clear that the spectra haven't color center and the absorption spectra are slightly shifter to longer wavelength with increasing SrO_2 content in the glasses. With help of UV–vis spectra in Fig. 4, the cut-off wavelength ($\lambda_{cut\text{-}off}$, nm) which necessary to calculate the optical absorption coefficient $\alpha(\lambda)$ was evaluated for each spectrum and written in Table 2. It seen that the value of $\lambda_{cut\text{-}off}$ increases with enhancement of SrO_2 content in the glasses, $\lambda_{cut\text{-}off}$ = 387, 404, 424, 445, 471, and 503 nm for BBPS0, BBPS5, BBPS10, BBPS15, BBPS20, and BBPS30 glasses, respectively.

In the present work, the optical absorption coefficients $\alpha(v)$ for each glass sample was estimated using the next relation via the absorbance (A) and sample thickness (d) [36]:

$$\alpha(v) = 2.303\left(\frac{A}{d}\right) = \left(\frac{1}{d}\right)\ln\left(\frac{I_o}{I}\right) \quad (7)$$

Tauc's model [37] depends on the optical absorption coefficient $\alpha(hv)$ was used to determine the allowed gaps for optical energy bands of the proposed glasses. This model modified by Mott and Davis as [38]:

$$\alpha(v)hv = \mathrm{C}(hv - E_{gap})^{\mathrm{m}}, \quad (8)$$

where the transition probability depends on the constant C. The power m points to the type of electronic transition (m = 2 and 0.5 for indirect and direct allowed transitions) [38]. The variation of $(\alpha h\nu)^2$ and $(\alpha h\nu)^{1/2}$ with photon energy (hv) for BBPS0–BBPS30 glasses are shown in Fig. 6a and b, respectively. The optical energy gaps in direct transition (E_{gap}^{Direct}) and for indirect transition ($E_{gap}^{Indirect}$) were determined with help of the linear region of the graphs at the points $(\alpha h\nu)^{1/2}$ or $(\alpha h\nu)^2 = 0$. All obtained values of E_{gap}^{Direct} and $E_{gap}^{Indirect}$ are collected in Table 2. Results reveal that the optical gap in both direct and indirect allowed shifts decrease with raising SrO_2 content in the prepared samples as shown in the inset figures of Fig. 6a and b, respectively. The values in case of direct allowed transition were changes between 3.15 eV for BBPS0 glass and 2.38 eV for BBPS30 sample, while 3.07 eV and 2.28 eV for BBPS30, respectively in case of direct allowable transition. Utilizing the values of E_{gap}^{Direct} and $E_{gap}^{Indirect}$, the average linear refractive on index (n) for all proposed glass samples was determined using the next relation [39, 40]:

$$\left(\frac{n^2-1}{n^2+2}\right) = 1 - \left(\frac{E_{gap}}{20}\right)^{0.5}. \quad (9)$$

The obtained n values are listed Table 2. The n changes from 2.368 for BBPS0 sample to 2.606 for

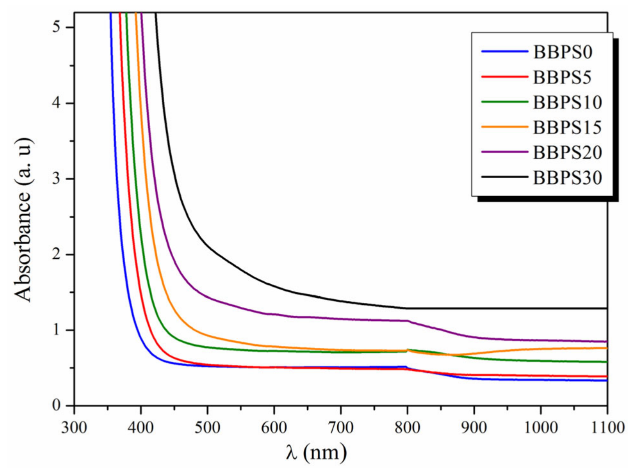

Fig. 5 Uv–Vis spectra for prepared BBPS0–BBPS30 glasses

Table 2 $\lambda_{cut\text{-}off}$, E_{gap}^{Direct}, $E_{gap}^{Indirect}$ Average (n), and E_U for BBPS0–BBPS30 glasses

Sample	$\lambda_{cut\text{-}off}$ (nm)	E (eV)		Average (n)	E_U (eV)
		Direct E_{gap}^{Direct}	Indirect $E_{gap}^{Indirect}$		
BBPS0	387	3.15	3.07	2.368	0.239
BBPS5	404	2.99	2.93	2.408	0.246
BBPS10	424	2.88	2.82	2.439	0.261
BBPS15	445	2.74	2.69	2.478	0.272
BBPS20	471	2.60	2.56	2.520	0.281
BBPS30	503	2.38	2.28	2.606	0.296

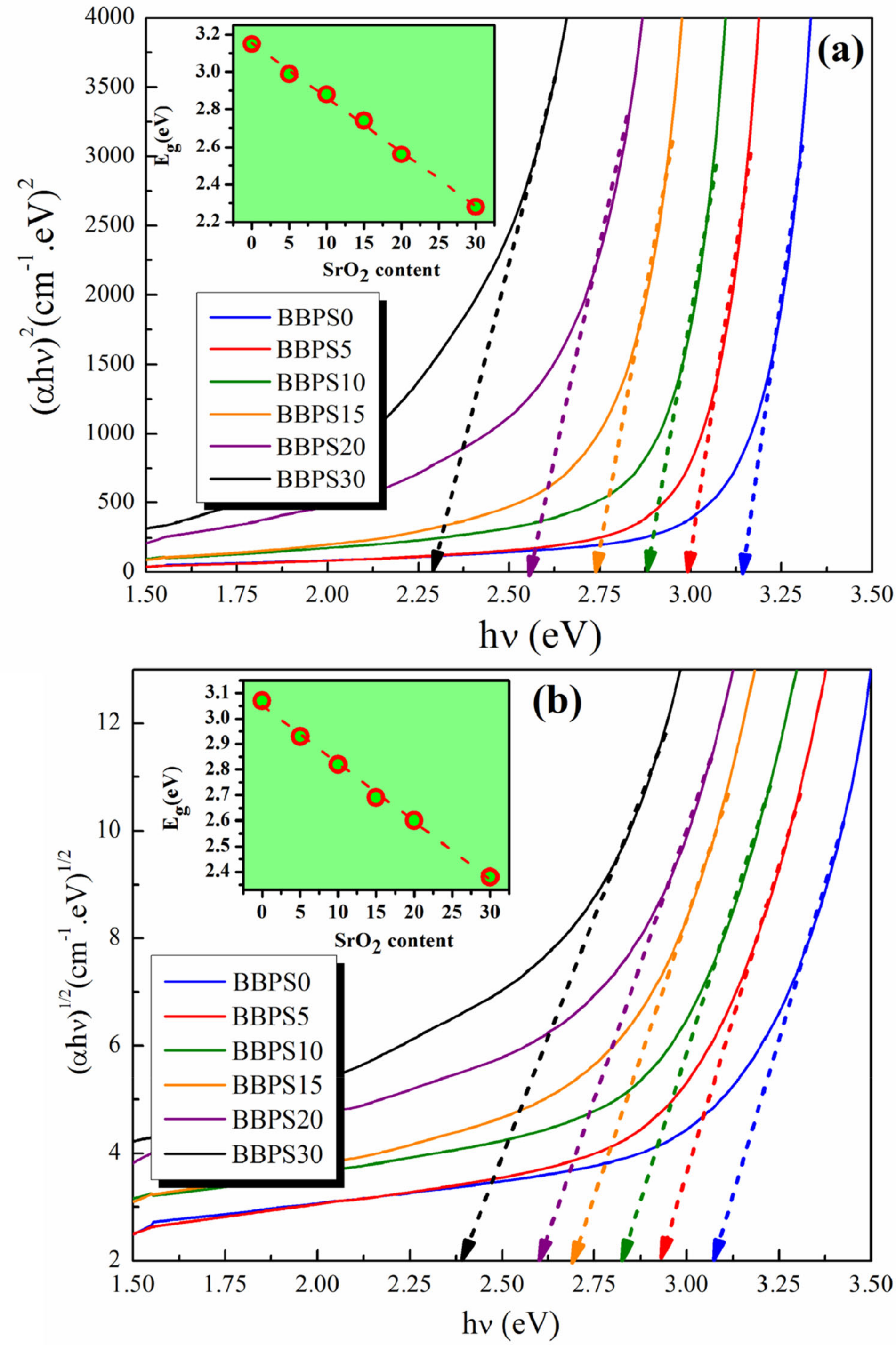

Fig. 6 Variation of **a** $(\alpha h\nu)^2$ and **b** $(\alpha h\nu)^{1/2}$ with $h\nu$ for BBPS0–BBPS30 glasses

BBPS30. Generally, n for the proposed glasses increase with enhancing SrO_2. Additionally, n is high, thus, the investigated glasses can be used as latent candidates in optical applications.

Urbach's energy (E_U) for all proposed glasses was calculated via the following relation [41]:

$$\alpha(\nu) = \bar{\alpha}(\nu) \exp\left(\frac{h\nu}{E_U}\right), \quad (10)$$

Here, $\bar{\alpha}(\nu)$ is a constant. By taking logarithm for both sides of Eq. (10) and drawing ln(α) versus ($h\nu$), the values of E_U can be obtained. The variation of ln(α) with $h\nu$ is shown in Fig. 7, from the linear part of

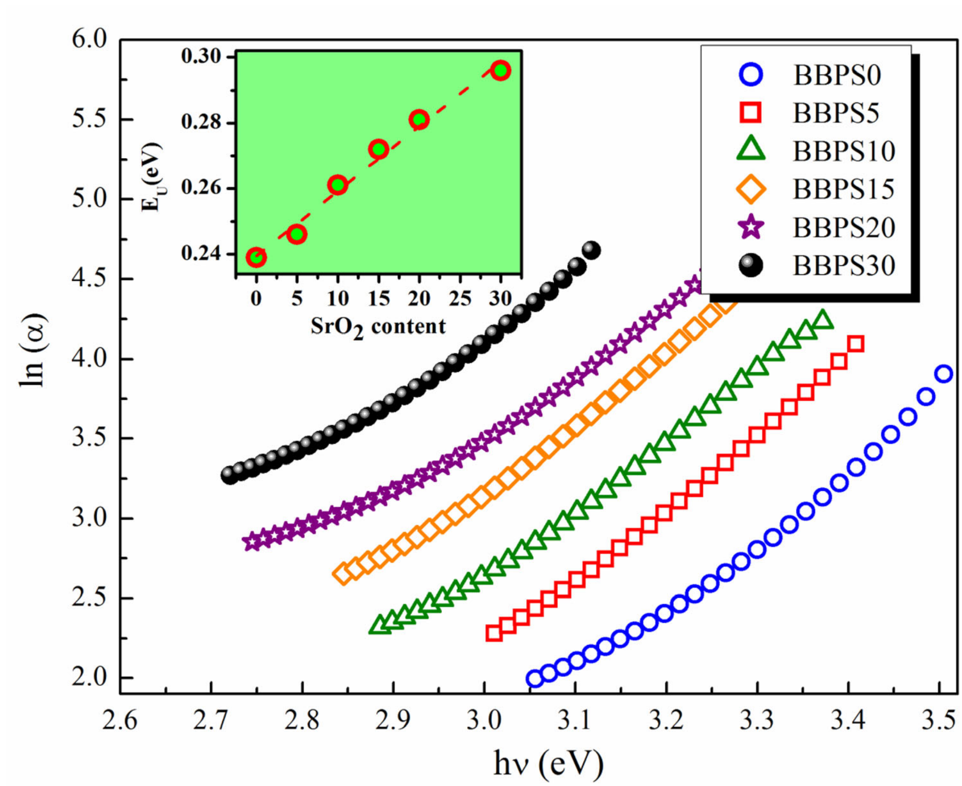

Fig. 7 Variation of ln(α) with *hν* for BBPS0–BBPS30 glasses

the curves, E_U values can be evaluated. E_U values recorded in Table 2 and plotted against SrO_2 content in the inset figure of Fig. 7. The increasing of E_U with increasing the amount of SrO_2 in the prepared glasses due to increase of localized state concentration in the bandgap.

3.3 Nuclear shielding competence

The mass attenuation coefficients-MAC values (μ_m) of the prepared glasses at the energy ranges are between 0.02 and 20 MeV were derived from MCNPX simulation code and WinXCOM. Table 3 shows these obtained MAC data. From Table 3, it can be seen that MCNPX and WinXCOM, data are in well agreement to each other. Therefore, obtained outcomes verifies that MCNPX simulation is accurate to compute the μ_m values [42, 43]. Figure 8 compares the results of MAC. It can be noted that MAC values of the studied glass materials (encoded BBPS0, BBPS5, BBPS10, BBPS15, BBPS20, BBPS30**)** are reflective to the variation in the energy levels. If photon energies approach 20 MeV, the MAC values begin to decrease. Among the glass samples examined, BBPS30 had the highest MAC values. In the other hand, HVL-MFP and TVL are critical parameters to consider when predicting the performance of investigated materials in shielding applications. It should be remembered that these parameters represent the materials' thickness. Figures 9, 10, and 11 illustrate the variations of HVL, TVL, and MFP values as a function of incident *hν*, respectively. Given the inverse relationship between HVL and μ (HVL = ln2/μ), it is reasonable to assume that the sample with the greatest values of μ can offer the lowest HVL values [44, 45]. This situation has been confirmed by our findings that BBPS30 sample was reported with the minimum HVL values among the investigated glasses. On the other hand, TVL has similar inverse relationship with μ values (TVL = ln10/μ) [46, 47]. As a result, a similar pattern was seen for the BBPS30 sample, with the lowest TVL values among the examined glasses. The term MFP refers to the average distance traveled by an electron throughout the scattering process. When all target particles are at rest except one, the MFP may be calculated using the average distance between the particles as MFP = 1/μ. The smallest MFP can be interpreted as an indication of gamma-ray attenuation supremacy, since it suggests that the incident photon's average moving distance is also the

Table 3 MAC ($\mu_m = \mu/\rho$) of the prepared glass system obtained from MCNPX and WinXCOM

Energy (MeV)	BBPS0		BBPS5		BBPS10		BBPS15		BBPS20		BBPS30	
	XCOM	MCNPX	XCOM	MCNPX	XCOM	MCNPX	XCOM	MCNPX	XCOM	MCNPX	XCOM	MCNPX
1.50E − 02	61.8079	62.6532	61.7102	62.3965	61.2236	62.3258	60.7548	61.6531	60.3029	61.1296	59.4462	60.259
2.00E − 02	41.4748	42.5124	44.0685	45.2651	45.3272	45.5874	46.5398	47.5624	47.7087	48.3654	49.9248	50.2654
3.00E − 02	14.4542	15.1624	15.3581	15.9824	15.7728	16.0047	16.1722	16.5427	16.5573	16.9657	17.2873	17.5952
4.00E − 02	13.1484	13.9542	12.4787	12.5103	12.5639	12.5869	12.6459	12.7652	12.7250	12.7824	12.8749	12.9124
5.00E − 02	7.3934	7.4126	7.0103	7.1069	7.0503	7.0769	7.0889	7.1004	7.1261	7.1306	7.1967	7.2114
6.00E − 02	4.6026	4.7024	4.3653	4.3713	4.3865	4.3926	4.4070	4.4126	4.4267	4.4317	4.4641	4.4721
8.00E − 02	2.1980	2.2214	2.0887	2.0988	2.0960	2.1069	2.1030	2.1128	2.1098	2.1239	2.1226	2.1328
1.00E − 01	2.7947	2.8136	2.8353	2.8421	2.8077	2.8124	2.7811	2.7923	2.7554	2.7596	2.7068	2.7158
1.50E − 01	1.0346	1.1062	1.0511	1.1121	1.0407	1.1001	1.0306	1.0501	1.0210	1.0368	1.0026	1.0224
2.00E − 01	0.5354	0.5396	0.5438	0.5441	0.5387	0.5391	0.5337	0.5342	0.5290	0.5293	0.5199	0.5212
3.00E − 01	0.2419	0.2432	0.2451	0.2462	0.2432	0.2436	0.2413	0.2116	0.2396	0.2401	0.2361	0.2386
4.00E − 01	0.1554	0.1561	0.1571	0.1579	0.1561	0.1569	0.1551	0.1560	0.1542	0.1548	0.1524	0.1532
5.00E − 01	0.1180	0.1193	0.1190	0.1195	0.1184	0.1188	0.1178	0.1185	0.1172	0.1175	0.1161	0.1167
6.00E − 01	0.0976	0.0992	0.0983	0.0986	0.0979	0.0982	0.0975	0.0979	0.0970	0.0975	0.0963	0.0769
8.00E − 01	0.0760	0.0771	0.0764	0.0768	0.0761	0.0764	0.0759	0.0761	0.0756	0.0759	0.0751	0.0755
1.00E + 00	0.0643	0.0654	0.0645	0.0653	0.0643	0.0650	0.0642	0.0650	0.0640	0.0649	0.0636	0.0640
1.50E + 00	0.0498	0.0512	0.0500	0.0513	0.0499	0.0513	0.0497	0.0515	0.0496	0.0515	0.0494	0.0516
2.00E + 00	0.0437	0.0453	0.0438	0.0453	0.0437	0.0454	0.0436	0.0454	0.0436	0.0455	0.0434	0.0456
3.00E + 00	0.0384	0.0390	0.0385	0.0391	0.0385	0.0392	0.0384	0.0392	0.0384	0.0393	0.0383	0.0394
4.00E + 00	0.0364	0.0371	0.0365	0.0372	0.0365	0.0373	0.0365	0.0374	0.0365	0.0375	0.0365	0.0376
5.00E + 00	0.0357	0.0363	0.0358	0.0363	0.0358	0.0365	0.0359	0.0366	0.0359	0.0367	0.0360	0.0368
6.00E + 00	0.0356	0.0360	0.0357	0.0361	0.0358	0.0363	0.0358	0.0365	0.0359	0.0366	0.0360	0.0366
8.00E + 00	0.0363	0.0365	0.0364	0.0366	0.0365	0.0367	0.0366	0.0369	0.0367	0.0371	0.0369	0.0372
1.00E + 01	0.0375	0.0381	0.0375	0.0382	0.0377	0.0385	0.0378	0.0387	0.0380	0.0388	0.0382	0.0389
1.50E + 01	0.0408	0.0412	0.0409	0.0414	0.0411	0.0415	0.0413	0.0417	0.0415	0.0419	0.0418	0.0420

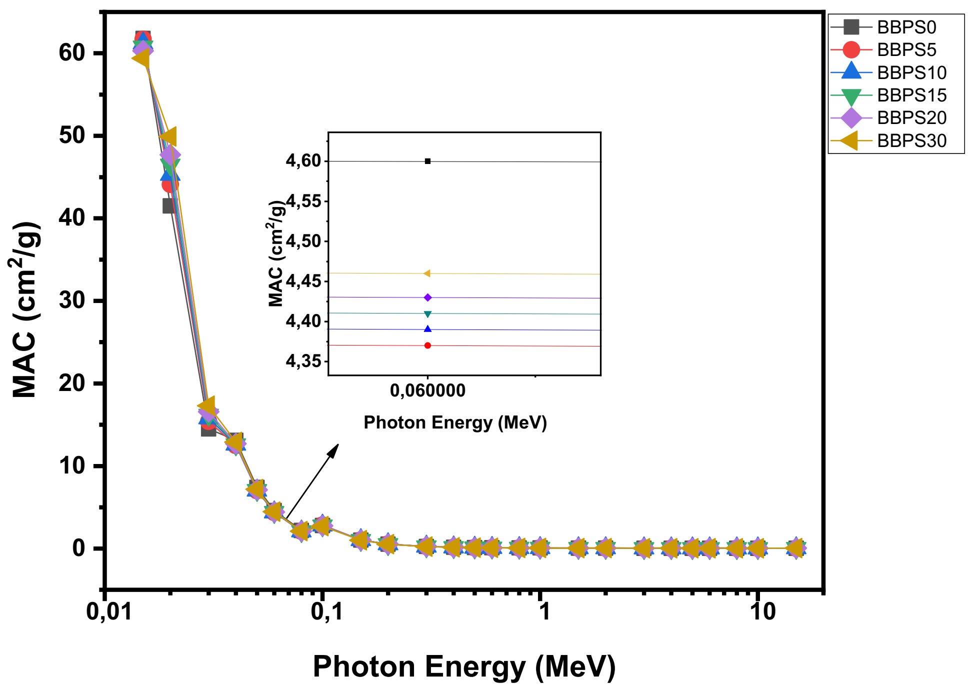

Fig. 8 Mass attenuation coefficient of the selected glasses with hv 0.02–20 MeV

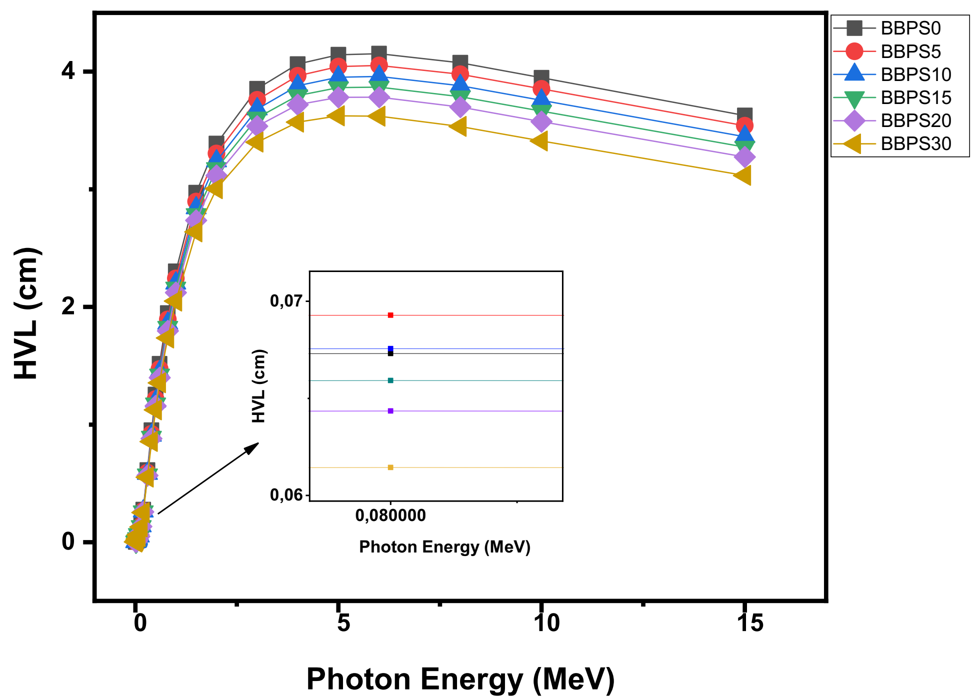

Fig. 9 HVL of the prepared glass samples

smallest. The results indicate that BBPS30 has the lowest MFP values at the photon energies studied. Overall, the findings list the HVL, MFP, and TVL values associated with each material in ascending order as BBPS0 > BBPS5 > BBPS10 > BBPS15 > BBPS20 > BBPS30. The various photons with B, C, O, Sr, Ba, Pb that derived from high Z dependency have a reducing impact on the HVL, MFP and TVL values. For example, while SrO_2 concentration in glass rise, HVLs for hv fall. The effective atomic numbers (Z_{eff}) values for the investigated glass sample with various SrO_2 concentration with respect to varying energy levels are reported in Fig. 12. From Fig. 12, possessing higher the Z_{eff} values, BBPS30 serves better in

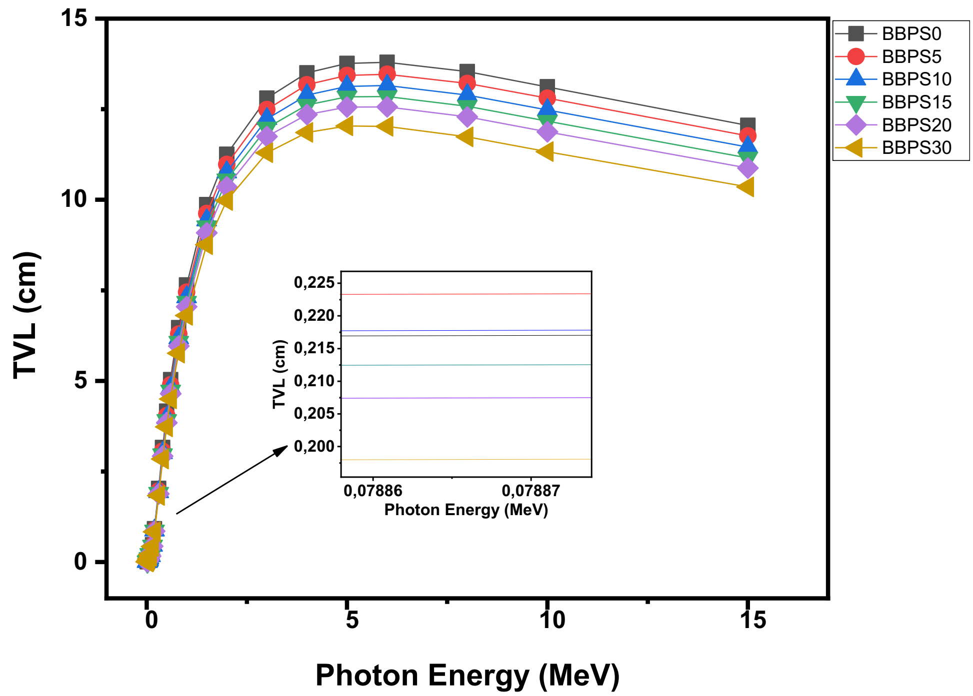

Fig. 10 TVL of the prepared glass samples

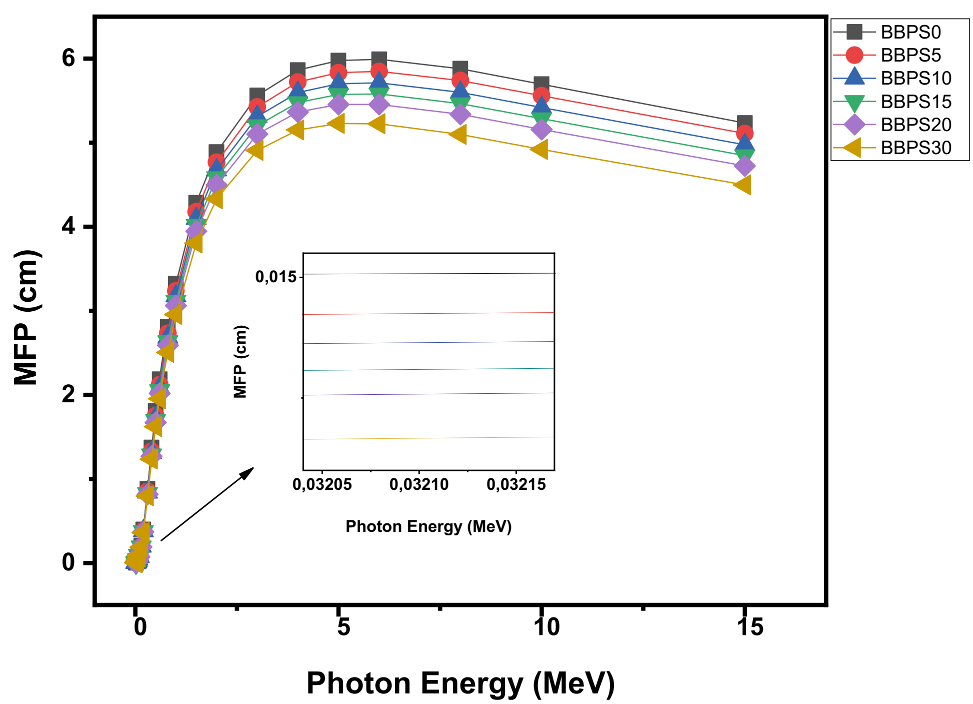

Fig. 11 MFP of the prepared glass samples

terms of radiation shielding [48–51]. The fast neutron effective removal cross-section values (ΣR) for BBPS0, BBPS5, BBPS10, BBPS15, BBPS20, BBPS30 samples are given in Fig. 13. It should be noted that ΣR decline with increasing SrO_2 concentration in the glass structure. The results show that the BBPS0 glass sample is better in terms of fast neutron shielding [19–22].

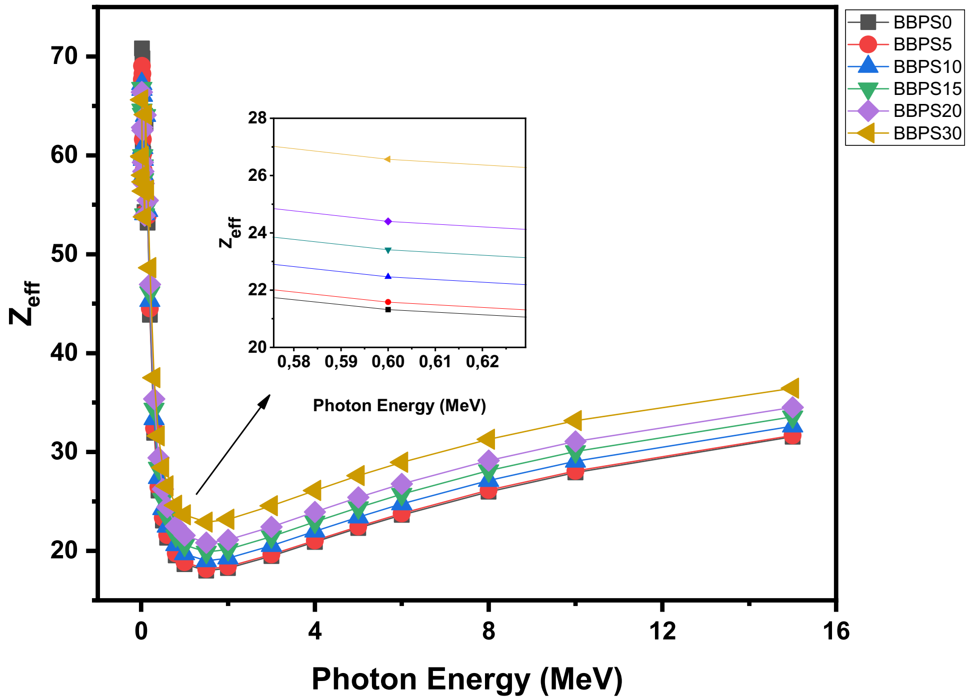

Fig. 12 Effective atomic numbers of the prepared glass samples with *hν*

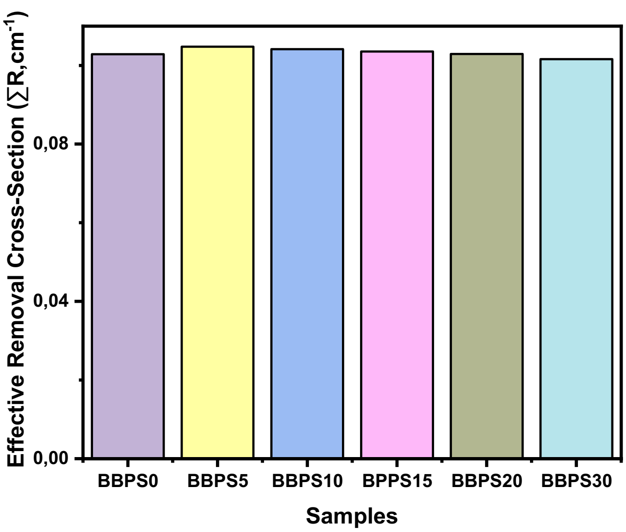

Fig. 13 Effective removal cross-section values of the glasses with density

4 Conclusion

The major aims of this work were to investigate the physical, UV–Vis–NIR spectroscopy and nuclear shielding properties of novel borate glasses with nominal compositions $50B_2O_3$–25BaO–25PbO–0SrO_2: x = 0–30 mol% (BBPS0–BBPS30). From the obtained results, one can concludes the following points:

1- Densities of the fabricated glasses increased from 4.685 to 5.315 g/cm^3, while molar volumes decreased from 29.869 to 29.152 cm^3/mol.
2- The non-crystalline nature of the fabricated glasses is confirmed by utilization of X-ray diffraction (XRD) measurements.
3- Direct and indirect (E_{gap}^{Direct}, $E_{gap}^{Indirect}$)optical energy gaps, average of refractive index (n), and Urbach's energy for (BBPS0–BBPS30) glasses were varied from varied from 3.15 to 2.38 eV, 3.07–2.28 eV, 2.268–2.606 eV, and 0.239–0.296 eV, respectively.
4- BBPS30 has maximum mass attenuation coefficient (μ/ρ) value which varies from 0.0420 to 60.259 cm^2/g for hν 0.015 and 15 MeV.
5- The HVL, MFP, and TVL values corresponding to the materials were in a descending order BBPS0 > BBPS5 > BBPS10 > BBPS15 > BBPS20 > BBPS30.
6- The $\sum$R decrease with increasing the density of glass samples.

Therefore, results confirm that BBPS30 glass has superior shielding features against gamma-rays than the other material in the studied sample of glasses.

Acknowledgements

Taif University Researchers Supporting Project number (Grant No. TURSP-2020/84), Taif University, Taif, Saudi Arabia.

References

1. A. Pan, A. Ghosh, Structural and optical properties of lithium bismuthate glasses. J. Mater. Res. **17**, 1941–1944 (2002)
2. P. Yasaka, N. Pattnaboonmee, H.J. Kim, P. Limkitjaroenporn, J. Kaewkhao, Gamma radiation shielding and optical properties measurements of zinc bismuth borate glasses. Ann. Nucl. Energy **68**, 4–9 (2014)
3. P. Becker, Borate materials in nonlinear optics. Adv. Mater. **10**, 979–992 (1998)
4. A.S. Abouhaswa, Y.S. Rammah, S.E. Ibrahim, A.A. El-Hamalawy, Structural, optical, and electrical characterization of borate glasses doped with SnO_2. J. Non-Cryst. Solids **494**, 59–65 (2018)
5. G. Jagannath, B. Eraiah, K. NagaKrishnakanth, S. Venugopal Rao, Linear and nonlinear optical properties of gold nanoparticles doped borate glasses. J. Non-Cryst. Solids **482**, 160–169 (2018)
6. S. Barbi, C. Mugoni, M. Montorsi, M. Affatigato, C. Gatto, C. Siligardi, Structural and optical properties of rare-earths doped barium bismuth borate glasses. J. Non-Cryst. Solids **481**, 239–247 (2018)
7. A.A. Ali, Y.S. Rammah, R. El-Mallawany, D. Souri, FTIR and UV spectra of pentaternary borate glasses. Measurement **105**, 72–77 (2017)
8. Y.S. Rammah, A.A. Ali, R. El-Mallawany, A.M. Abdelghany, Optical properties of bismuth borotellurite glasses doped with $NdCl_3$. J. Mol. Struct. **1175**, 504–511 (2019)
9. Y.S. Rammah, A.S. Abouhaswa, M.I. Sayyed, H.O. Tekin, R. El-Mallawany, Structural, UV and shielding properties of ZBPC glasses. J. Non-Cryst. Solids **509**, 99–105 (2019)
10. Y.S. Rammah, M.I. Sayyed, A.S. Abohaswa, H.O. Tekin, FTIR, electronic polarizability and shielding parameters of B_2O_3 glasses doped with SnO_2. Appl. Phys. A **124**, 650 (2018)
11. Y.S. Rammah, M.I. Sayyed, A.A. Ali, H.O. Tekin, R. El-Mallawany, Optical properties and gamma-shielding features of bismuth borate glasses. Appl. Phys. A **124**, 832 (2018)
12. Y.S. Rammah, A.S. Abouhaswa, A.H. Salama, R. El-Mallawany, Optical, magnetic characterization, and gamma-ray interactions for borate glasses using XCOM program. J. Theor. Appl. Phys. **13**, 155–164 (2019)
13. A. Terczynska-Madej, K. Cholewa-Kowalska, M. Łaczka, J. Opt. Mater. **33**, 12 (2011)
14. U. Hoppe, R. Kranold, A. Ghosh, C. Landron, J. Neuefeind, P. Jovari, Environments of lead cations in oxide glasses probed by X-ray diffraction. J. Non-Cryst. Solids **328**, 146 (2003)
15. V. Martin, B. Wood, U. Werner-Zwanziger, J. Zwanziger, Structural aspects of the photoelastic response in lead borate glasses. J. Non-Cryst. Solids **357**, 2120 (2011)
16. Z. Pan, S. Morgan, B. Long, Raman scattering cross-section and non-linear optical response of lead borate glasses. J. Non-Cryst. Solids **185**, 127 (1995)
17. T. Takaishi, J. Jin, T. Uchino, T. Yoko, Structural study of PbO–B2O3 glasses by X-ray diffraction and ^{11}B MAS NMR techniques. J. Am. Ceram. Soc. **83**, 2543 (2000)
18. N. Manikandan, A. Ryasnyanskiy, J. Toulouse, Thermal and optical properties of TeO_2–ZnO–BaO glasses. J. Non-Cryst. Solids **358**, 947–951 (2012)
19. N. Elkhoshkhany, H.M. Mohamed, E. Yousef, UV–Vis-NIR spectroscopy, structural and thermal properties of novel oxyhalide tellurite glasses with composition TeO_2–B_2O_3–$SrCl_2$–LiF–Bi_2O_3 for optical application. Results in Physics **13**, 102222 (2019)
20. N. Chantima, J. Kaewkhao, P. Limsuwan, Study of photon interactions and shielding properties of silicate glasses containing Bi_2O_3, BaO and PbO in the energy region of 1 keV to 100 GeV. Ann. Nucl. Energy **41**, 119–124 (2012)
21. S. Kaewjaeng, U. Maghanemi, S. Kothan, H.J. Kim, P. Limkitjaroenporn, J. Kaewkhao, New gadolinium based glasses for gamma-rays shielding materials. Nucl. Eng. Design **280**, 21–26 (2014)
22. S. Kaewjaeng, J. Kaewkhao, P. Limsuwan, U. Maghanemi, Effect of BaO on optical, physical and radiation shielding properties of SiO_2–B_2O_3–Al_2O_3–Na_2O glass system. Proced. Eng. **32**, 1080–1086 (2012)
23. M.S. Al-Buriahi, A.S. Abouhaswa, H.O. Tekin, C. Sriwunkum, F.I. El-Agawany, T. Nutaro, E. Kavaz, Y.S. Rammah, Structure, optical, gamma-ray and neutron shielding properties of NiO doped B_2O_3–$BaCO_3$–Li_2O_3 glass systems. Ceram. Int. **46**, 1711–1721 (2020)
24. M.S. Al-Buriahi, Y.S. Rammah, Investigation of the physical properties and gamma-ray shielding capability of borate glasses containing PbO, Al_2O_3 and Na_2O. Appl. Phys. A **125**, 717 (2019)
25. M.S. Al-Buriahi, B.T. Tonguc, Study on gamma-ray buildup factors of bismuth borate glasses. Appl. Phys. A **125**, 482 (2019)
26. Y.S. Rammah, M.S. Al-Buriahi, A.S. Abouhaswa, B_2O_3–$BaCO_3$–Li_2O_3 glass system doped with CO_3O_4: structure,

optical, and radiation shielding properties. Phys. B **576**, 411717 (2019)

27. Y.S. Rammah, A. Askin, A.S. Abouhaswa, F.I. El-Agawany, M.I. Sayyed, Synthesis, physical, structural and shielding properties of newly developed B_2O_3–ZnO–PbO–Fe_2O_3 glasses using Geant4 code and WinXCOM program. Appl. Phys. A **125**, 523 (2019)
28. M.I. Sayyed, I.A. El-Mesady, A.S. Abouhaswa, A. Askin, Y.S. Rammah, Comprehensive study on the structural, optical, physical and gamma photon shielding features of B_2O_3–Bi_2O_3–PbO–TiO_2 glasses using WinXCOM and Geant4 code. J. Mol. Struct. **1197**, 656–665 (2019)
29. Y. Al-Hadeethi, M.I. Sayyed, Y.S. Rammah, Investigations of the physical, structural, optical and gamma-rays shielding features of B_2O_3–Bi_2O_3–ZnO–CaO glasses. Ceram. Int. **45**, 20724–20732 (2019)
30. E. Şakar, Ö.F. Özpolat, B. Alım, M.I. Sayyed, M. Kurudirek, Phy-X/PSD: development of a user friendly online software for calculation of parameters relevant to radiation shielding and dosimetry. Radiat. Phys. Chem. **166**, 108496 (2020)
31. Ö.F. Özpolat, B. Alım, E. Şakar, M. Büyükyıldız, M. Kurudirek, Phy-X/ZeXTRa: a software for robust calculation of effective atomic numbers for photon, electron, proton, alpha particle, and carbon ion interactions. Radiat. Environ. Biophys. **59**, 321–329 (2020). https://doi.org/10.1007/s00411-019-00829-7
32. MCNPX 240, Monte Carlo N-Particle transport code system for multiparticle and high energy applications (Sep 2004). Available on-line: http://www.nea.fr/abs/html/ccc-0715.html
33. V. Mosorov, The Lambert–Beer law in time domain form and its application. Appl. Radiat. Isot. **128**, 1–5 (2017)
34. L. Gerward, N. Guilbert, K.B. Jensen, H. Levring, WinXCom—a program for calculating X-ray attenuation coefficients. Radiat. Phys. Chem. **71**, 653–654 (2004)
35. F. Akman, R. Durak, M.F. Turhan, M.R. Kaçal, Studies on effective atomic numbers, electron densities from mass attenuation coefficients near the K edge in some samarium compounds. Appl. Rad. Iso. **101**, 107–113 (2015)
36. D.A. Rayan, Y.H. Elbashar, M.M. Rashad, A. El-Korashy, Spectroscopic analysis of phosphate barium glass doped cupric oxide for bandpass absorption filter. J. Non Cryst. Solids **382**, 52–56 (2013)
37. J. Tauc (ed.), *Amorphous and Liquid Semiconductors* (Plenum Press, New York, 1974)
38. N.F. Mott, E.A. Davies, *Electronic Processes in Non-Crystalline Materials* (Clarendon Press, Oxford, 1979)
39. V. Dimitrov, S. Sakka, Electronic oxide polarizability and optical basicity of simple oxides. J. Appl. Phys. **79**, 1736–1740 (1996)
40. R. El-Mallawany, M.D. Abdalla, I.A. Ahmed, New tellurite glasses, optical properties. Mater. Chem. Phys **109**, 291–296 (2008)
41. F. Urbach, Phys. Rev. **92**, 1324 (1953)
42. H.O. Tekin, T.T. Erguzel, M. Karahan, U. Kara, O. Kilicoglu, A. Mesbahi, M.I. Sayyed, Investıgatıon of water equivalance and shielding properties of different solid phantoms using MCNPX code. Dig. J. Nanomater. Biostruct. **13**, 9 (2018)
43. H.O. Tekin, M.I. Sayyed, O. Kilicoglu, M. Karahan, T.T. Erguzel, U. Kara, M. Konuk, Calculation of gamma-ray attenuation properties of some antioxidants using Monte Carlo simulation method. Biomed. Phys. Eng. Express. **4**, 057001 (2018)
44. O. Agar, E. Kavaz, E.E. Altunsoy, O. Kilicoglu, H.O. Tekin, M.I. Sayyed, T.T. Erguzel, N. Tarhan, Er2O3 effects on photon and neutron shielding properties of TeO_2–Li_2O–ZnO–Nb_2O_5 glass system. Res. Phys. **13**, 102277 (2019). https://doi.org/10.1016/j.rinp.2019.102277
45. M.G. Dong, O. Agar, H.O. Tekin, O. Kilicoglu, K.M. Kaky, M.I. Sayyed, A comparative study on gamma photon shielding features of various germanate glass systems. Compos. B **165**, 636–647 (2019)
46. M.I. Sayyed, H.O. Tekin, O. Kılıcoglu, O. Agar, M.H.M. Zaid, Shielding features of concrete types containing sepiolite mineral: comprehensive study on experimental XCOM and MCNPX results. Res. Phys. **11**, 40–45 (2018). https://doi.org/10.1016/j.rinp.2018.08.029
47. S.A.M. Issa, Y.B. Saddeek, M.I. Sayyed, H.O. Tekin, O. Kilicoglu, Radiation shielding features using MCNPX code and mechanical properties of the $PbONa_2OB_2O_3CaOAl_2O_3$-SiO_2 glass systems. Compos. B **167**, 231–240 (2019). https://doi.org/10.1016/j.compositesb.2018.12.029
48. H.O. Tekin, O. Kilicoglu, E. Kavaz, E.E. Altunsoy, M. Almatari, O. Agar, M.I. Sayyed, The investigation of gamma-ray and neutron shielding parameters of Na_2O–CaO–P_2O_5–SiO_2 bioactive glasses using MCNPX code. Res. Phys. **12**, 1797–1804 (2019). https://doi.org/10.1016/j.rinp.2019.02.017
49. S.A. Issa, H.O. Tekin, R. Elsaman, O. Kilicoglu, Y.B. Saddeek, M.I. Sayyed, Radiation shielding and mechanical properties of Al_2O_3–Na_2O–B_2O_3–Bi_2O_3 glasses using MCNPX Monte Carlo code. Mater. Chem. Phys. **223**, 209–219 (2019). https://doi.org/10.1016/j.matchemphys.2018.10.064
50. I.S. Mahmoud, S.A. Issa, Y.B. Saddeek, H.O. Tekin, O. Kilicoglu, T. Alharbi, M.I. Sayyed, T.T. Erguzel, R. Elsaman, Gamma, neutron shielding and mechanical parameters for lead vanadate glasses. Ceram. Int. **45**, 14058–14072 (2019). https://doi.org/10.1016/j.ceramint.2019.04.105
51. O. Kilicoglu, Characterization of copper oxide and cobalt oxide substituted bioactive glasses for gamma and neutron

shielding applications. Ceram. Int. **45**, 23619–23631 (2019). https://doi.org/10.1016/j.ceramint.2019.08.073

Publisher's Note Springer Nature remains neutral with regard to jurisdictional claims in published maps and institutional affiliations.